Simulating Photovoltaic Array Performance with Solar Radiation Observations from the Oklahoma Mesonet

Nicholas A. Engerer and Mark Morrissey

School of Meteorology, University of Oklahoma

1. Introduction

Sixteen years (1994-2009) of global horizontal radiation measurements were obtained from the Oklahoma Mesonet (Brock, Crawford et al. 1995). Data points were available at five-minute increments for 108 different stations, and were extensively quality controlled. For this study, more than 90 million solar radiation observations were ingested into a computer code consisting of radiation, photovoltaic and inverter models in order to obtain estimates of photovoltaic array output in kilowatt-hours.

The purpose of this study is to provide estimates of energy production from 2kW rooftop sized photovoltaic arrays in order to encourage photovoltaic installations in the state of Oklahoma.

2. Methodology

2.1 Mesonet Observations

Oklahoma Mesonet solar radiation observations are obtained from LI200S Li-Cor pyranometers (Campbell-Scientific 1996). These pyranometers feature a high stability silicon sensor that samples light between 400-1100 nm in wavelength and are accurate to within +-3%. Mesonet observations are reported as 5 minute averages of global solar radiation, restricted to the skyward hemisphere (Brock, Crawford et al. 1995).

2.2 Solar Radiation Overview

The shortwave solar radiation measured by the Mesonet pyranometers arrives in two distinct forms. The first is direct or *beam* radiation, which arrives at the sensor without having been scattered by the atmosphere. The second form is diffuse radiation, which is received by the sensor after being scattered by air molecules (Rayleigh Scattering), aerosols and water vapor. No distinction is made between these two components in the reported observations. However, in order to predict the amount of radiation incident upon a tilted photovoltaic module surface, the provided global radiation measurement must first be separated into direct and diffuse components and then these components must be transposed to the given tilt angle. Both of these processes are accomplished via radiation models.

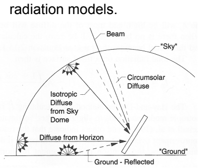

Fig 1: An image showing the sources of radiation impinging upon titled modules. Beam radiation arrives in a direct path from the sun, while diffuse radiation arrives indirectly after being scattered by air molecules, clouds or aerosols. Image courtesy of Duffie 2006.

2.3 Maxwell Separation Model

Citing its superiority over other separation models (Gueymard 2009), the Maxwell Separation Model (Maxwell 1987) was chosen to separate the global horizontal radiation measurements used in this study. The first step in the modeling process is calculation of the clearness index K_t from the observed global horizontal radiation observation E_g and the extraterrestrial radiation E_{ext} estimated by Duffie 2006 (equation a).

Next, the clear sky clearness index K_n is introduced. This index is given by the ratio between direct normal irradiance E_n and the extraterrestrial radiation, E_{ext} (b). This direct normal irradiance (DNI) value is required for the needed separation.

To solve for DNI, Maxwell 1987 empirically establishes a relationship for the calculation of the limiting value of the clear sky clearness condition K_{nc} (c) and the current departure from this limiting value, ΔK_n (d) through a least-squares regression analysis of data collected in Atlanta in 1981. Where calculation of the relative air mass is given by (e) and z is the zenith angle of the sun

In this manner, through the relationship of the clear sky clearness index, the clear sky clearness index limiting value and the current departure value is given by (f). Finally, using the clear sky clearness index, direct normal irradiance E_n can be calculated from (g).

Equations in Maxwell 1987

$$\text{(a) } K_t = E_g/Eext \qquad \text{(b) } Kn = E_n/E_{ext}$$
$$\text{(c) } K_{nc} = 0.866 - 0.122\cdot AM + 0.0121\cdot (AM)^2 - 0.000653\cdot (AM)^3 + 0.000014\cdot (AM)^4$$
$$\text{(d) } \Delta K_n = a + b \cdot \exp(c \cdot AM)$$
$$\text{(e) } AM = \{\cos(z) + 0.5057\cdot (96.08 - z)^{-1.634}\}^{-1.0} \dagger$$
$$\text{(f) } K_n = K_{nc} - \Delta K_n \qquad \text{(g) } E_n = E_{ext} \cdot K_n$$

2.4 Separation of Global Measurements

The provided estimate of DNI from the Maxwell Separation model allows estimation of the horizontal component of beam radiation (E_{bh}) and beam radiation at module tilt (E_b) from equations provided by (Duffie 2006) (h and i). Where θ is the angle of incidence of beam radiance on the module (j). The tilt of the module is given as α_m and the azimuth orientation by γ_m. The azimuth of the sun is γ.

Calculation of the horizontal diffuse radiation component is now straightforward and is found in equations (k) and (m).

An estimate of diffuse radiation received on the tilted module surface is the final component required, and requires a radiation transposition model.

Separation Equations

$$\text{(h) } E_{bh} = E_n \cdot\cos(z) \qquad \text{(i) } E_b = E_{n-} \cdot \cos(\theta)$$
$$\text{(j) } \cos(\theta) = \cos(\alpha_m) \cdot\cos(z) + \sin(\alpha_m) \cdot\sin(z) \cdot\cos(\gamma-\gamma_m)$$
$$\text{(k) } E_g = E_{bh} + E_{dh} \qquad \text{(m) } E_{dh} = E_{bh} - E_g$$

2.5 HDKR Transposition Model

Tilted modules receive diffuse radiation from several sources: *isotropic* radiation emitted by the entire sky hemisphere, *circumsolar* diffuse radiation surrounding the sun and *horizon brightening* radiation emanating from the edges of the sky. Through the evaluation of 10 transposition models by Gueymard 2009, the Reindl Transposition model (Reindl, Beckman et al. 1990) was selected for use in this study. This model is also known as the HDKR model (Hay, Davies, Klucher, Reindl citing contributions from (Hay 1979; Klucher 1979)).

The diffuse fraction of radiation at module tilt is given by the Reindl transposition model as (n). Where A_i is the *anisotropy index* (equivalent to K_t defined in Maxwell model). R_b is the geometric factor, defined in Duffie 2006 as (o). *f* is a modulating factor, and serves to reduce the horizon brightening effect as cloudiness increases (Klucher 1979) and is given (p):

HDKR Model

$$\text{(n) } E_d = E_{dh} \cdot \{(1 - A_i) \cdot 0.5\cdot (1+\cos(\alpha_m) \cdot \{1 + f\cdot\sin^3(\alpha_m/2)\} + A_i\cdot R_b\}$$
$$\text{(o) } R_b = \cos(\theta)/\cos(z) \qquad \text{(p) } f = \sqrt{}E_{bh}/E_g$$

2.6 Photovoltaic Simulation through the Sandia Performance Model

The Sandia Performance Model (King 2004) was developed at Sandia National Laboratories over a twelve year period from 1992-2004. The model predicts photovoltaic array performance to a high degree of accuracy (B. Kroposki 2000) from input meteorological data, using empirically determined electrical, thermal and optical parameters specific to individual module types. These are provided by the Sandia Performance Model (SPM) database, which includes simulation data for over 500 module types from the years 1994 through 2010, and was compiled through outdoor performance testing.

2.6.1 Basic Equations

Although the SPM can reproduce five points on the I-V Power Curve, only the maximum power point, P_{mp}, will be calculated in this study. Deviation from this point on the power curve is uncommon for grid-tied photovoltaic modules, as the voltage and current levels are held steady by incoming power from the electric grid (Engerer 2010).

In order to calculate P_{mp}, the voltage at maximum power V_{mp} and the current at maximum power I_{mp} are required, and are given by (q) and (r). P_{mp} is then calculated by (s).

Basic Equations

$$\text{(q) } I_{mp} = I_{mpo} \cdot\{C0\cdot E_e + C1\cdot E_e^2\}\cdot\{1 + \alpha_{Imp}\cdot(T_c-T_o)\}$$
$$\text{(r) } V_{mp} = V_{mpo} + C2\cdot N_s\cdot\delta(Tc)\cdot\ln(E_e) + C_3\cdot N_s\cdot\{\delta(T_c)\cdot\ln(E_e)\}^2 + \beta_{Vmp}(E_e)\cdot(T_c-T_o)$$
$$\text{(s) } P_{mp} = I_{mp}\cdot V_{mp}$$

T_c = Module temp.
T_o = Reference. cell temp, typically 25°C
E_o = Ref. irradiance, typically 1000 W/m²
$\delta(T_c)$ = 'Thermal voltage' at Tc
N_s = # cells in series in module cell-string
$\beta_{Vmp}(E_e) = \beta_{Vmpo} + m_{\beta Vmp}\cdot(1-E_e)$,
Temp. coefficient for module max-power-voltage
I_{mpo} = Current at P_{mp} at T_o, E_o
V_{mpo} = Voltage at P_{mp} at T_o, E_o
C_0, C_1 = Empirical coefficients relating I_{mp} to E_e
C_2, C_3 = Empirical coefficients relating V_{mp} to E_e

2.6.2 Calculation of Effective Radiation E_e

To prepare the radiation measurements for ingestion into the SPM, effective radiation E_e must be calculated according to (t). The equation provides the portion of the total radiation incident on the module surface that will be used by the module for energy production. It accounts for variation in the solar spectrum as a function of absolute air mass (u) through the empirical function $f_1(AM_a)$ (v) as well as for optical losses incurred by θ, the angle of incidence in $f_2(\theta)$ (w). These functions were developed through outdoor testing of relevant modules (King 1997). The coefficients, a_0, a_1, a_2, a_3, a_4 and b_0, b_1, b_2, b_3, b_4 are module specific and provided in the Sandia Module Database.

Effective Radiation

$$\text{(t) } E_e = f_1(AM_a)\cdot\{(E_b\cdot f2(\theta)+f_d\cdot E_d) / E_o\}\cdot SF$$
$$\text{(u) } f_1(AM_a) = a_0 + a_1\cdot AM_a + a_2\cdot(AM_a)^2 + a_3\cdot(AM_a)^3 + a_4\cdot(AM_a)^4$$
$$\text{(v) } f2(\theta) = b_0 + b_1\cdot\theta + b_2\cdot(\theta)^2 + b_3\cdot(\theta)^3 + b_4\cdot(\theta)^4 + b_5\cdot(\theta)^5$$
$$\text{(w) } AM_{a-} = AM\cdot\exp(-0.0001184\cdot\eta)$$

η = station elevation in meters
SF = soiling factor

2.7 Information about Simulated Arrays

Through correspondence with Sunrise Alternative Energy, a renewable energy company that performs solar installs in Oklahoma, the following rooftop array designs were chosen to be simulated:

Module Type	Sharp ND-216U1F	Sanyo HIP-200BA3
# in Series	5	5
# in Parallel	2	5
Inverter	Xantrex GT2.8	Fronius IG2000
Rating (W)	2160	2000

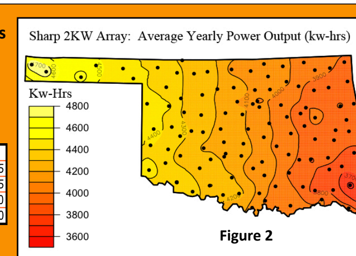

Figure 2

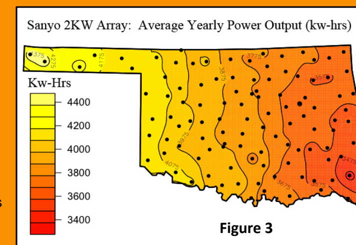

Figure 3

3. Preliminary Results

After integrating the SPM forward at 5 minute time increments over 16 years of data, averages of yearly totals were created for each of the 108 stations. Data were spatially de-trended in order to consider the general increase in terrain and aridity (fewer clouds) associated with westward movement across the state. The creation of sample variograms and subsequent variogram modeling followed. The averages were then interpolated spatially via Ordinary Kriging (Isaaks and Srivastava) using 35 neighbor stations. The resulting maps for the Sharp array and Sanyo array are presented in figures 2 and 3, respectively.

3.1 Monthly Energy Production

Monthly energy production values from the Sharp 2kW array for the Mt. Herman and Kenton stations (minimum and maximum yearly production respectively) are provided in figures 4 and 5.

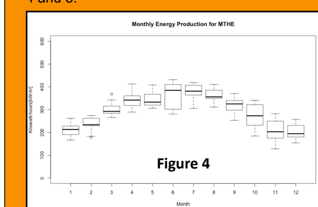

Figure 4

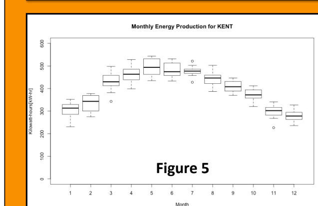

Figure 5

3.2 Expressing Potential Variability

Additionally, values of the first standard deviation were analyzed and kriged to produce the maps in figures 6 and 7 in order to provide users with the expected variation from the average yearly power production values.

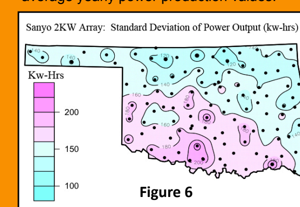

Figure 6

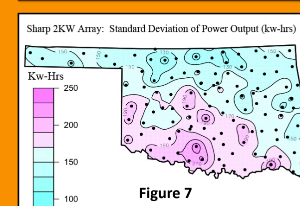

Figure 7

Acknowledgments

This project was made possible by graduate fellowship funding provided by the American Society for Engineering Education through the National Defense Science and Engineering Graduate Fellowship. Additional gratitude is due to the Oklahoma Climate Survey and the Oklahoma Mesonet, without such resources this project would not be possible.

References

B. Kroposki, W. M., D. King, W. Boyson, and J. Kratochvil (2000). Comparison of Module Performance Characterization Methods. 28th IEEE PV Specialists Conference: 1407-1411.
Brock, F. V., K. C. Crawford, et al. (1995). "The Oklahoma Mesonet: A Technical Overview." Journal of Atmospheric and Oceanic Technology **12**(1): 5-19.
Campbell-Scientific (1996). LI200S Instruction Manual. Logan, UT, Campbell Scientific.
Duffie, J. A. a. W. A. B. (2006). Solar Energy Thermal Processes. New York, NY, Wiley Interscience.
Engerer, D. P. E. S. E., Distribution Planning and Protection (2010). Personal Communication. Akron, OH, FirstEnergy Corp.
Gueymard, C. A. (2009). "Direct and indirect uncertainties in the prediction of tilted irradiance for solar engineering applications." Solar Energy **83**(3): 432-444.
Hay, J. E. (1979). "Calculation of monthly mean solar radiation for horizontal and inclined surfaces." Solar Energy **23**(4): 301-307.
Isaaks, E. H. and R. M. Srivastava An Introduction to Applied Geostatistics, Oxford University Press.
King, D. L., W. E. Boyson, et al. (1997). Improved accuracy for low-cost solar irradiance sensors. Conference: 2. world conference and exhibition on photovoltaic solar energy conversion, Vienna (Austria), 6-10 Jul 1998; Other Information: PBD: [1997]: Medium: ED; Size: 4 p.
King, D. L., J. Kratochvil and W. Boyson (1997). Measuring Solar Spectral and Angle-of-Incidence Effects on PV Modules and Solar Irradiance Sensors. 26th IEEE PV Specialists Conference: 1113-1116.
King, D. L., W.E. Boyson, J.A. Kratochvil (2004). Photovoltaic Array Performance. S. N. Laboratories. Albuquerque, NM. **SAND2004-3535**.
Klucher, T. M. (1979). "Evaluation of models to predict insolation on tilted surfaces." Solar Energy **23**(2): 111-114.
Maxwell, E. L. (1987). Quasi-physical model for converting hourly global horizontal to direct normal insolation. Solar '87 Conference, Portland, OR, American Solar Energy Society.
Perez, R., P. Ineichen, et al. (1990). "Modeling daylight availability and irradiance components from direct and global irradiance." Solar Energy **44**(5): 271-289.
Reindl, D. T., W. A. Beckman, et al. (1990). "Evaluation of hourly tilted surface radiation models." Solar Energy **45**(1): 9-17.